GeoVirtual 2020 September 14-16
Resilience and Innovation

Assessment of pipelines subjected to varying longitudinal soil displacement rates

Chee K. Wong[1], Richard G. Wan[2] & Ron C.K. Wong[2]
[1]Research Associate, Department of Civil Engineering – University of Calgary, Calgary, AB, Canada
[2]Professor, Department of Civil Engineering – University of Calgary, Calgary, AB, Canada

ABSTRACT
A number of oil and gas pipelines have been constructed and buried at shallow depths across slopes in the province of Alberta, Canada. Due to complex terrains and geological formations, these slopes are active, continually moving in varying rates. Pipeline sections subjected to such permanent long-term ground deformations may yield because of large strain accumulation over time. It is of practical importance to quantify how such movement rates affect the integrity of the pipe so that an effective field monitoring and remediation program can be developed to maintain the integrity and prolong its operation. In the past, solutions have been developed for analysis of buried pipes under axial (longitudinal) loading due to translational slides. These solutions do not consider the effect of soil displacement rate on (i) excess pore pressure responses (generation and dissipation) around the pipe and (ii) soil-pipe interface behaviour. This paper develops simplified semi-analytical solutions to characterize this coupled phenomenon in soil-pipe interaction under axial (longitudinal) loading and to estimate the strains exerted on a pipe subjected to varying soil displacement rates. These solutions will be used in a case study to assess the potential of yielding in the pipe with the given soil displacement rates that occurred in the slope.

RÉSUMÉ
Un certain nombre d'oléoducs et de gazoducs ont été construits et enfouis à faible profondeur sur les pentes de la province de l'Alberta, au Canada. En raison de terrains complexes et de formations géologiques, ces pentes sont actives et se déplacent continuellement à des taux variables. Les sections de pipelines soumises à de telles déformations permanentes du sol à long terme peuvent céder en raison d'une forte accumulation de déformation au fil du temps. Il est d'une importance pratique de quantifier la manière dont ces taux de mouvement affectent l'intégrité de la conduite afin qu'un programme efficace de surveillance sur le terrain et d'assainissement puisse être développé pour maintenir l'intégrité et prolonger son fonctionnement. Dans le passé, des solutions ont été développées pour l'analyse des tuyaux enterrés sous une charge axiale (longitudinale) due aux glissières de translation. Ces solutions ne tiennent pas compte de l'effet du taux de déplacement du sol sur (i) les réponses de pression interstitielle excessive (génération et dissipation) autour du tuyau et (ii) le comportement de l'interface sol-tuyau. Cet article développe des solutions semi-analytiques simplifiées pour caractériser ce phénomène couplé dans l'interaction sol-tuyau sous charge axiale (longitudinale) et pour estimer les déformations exercées sur un tuyau soumis à des taux de déplacement du sol variables. Ces solutions seront utilisées dans une étude de cas pour évaluer le potentiel de céder dans le tuyau avec les taux de déplacement du sol donnés qui se sont produits dans la pente.

1 INTRODUCTION

Buried pipelines are used for transport of natural resources, such as water, oil, and natural gas. On account of circumstances in difficult terrains, pipelines sometimes are laid in slopes which are commonly subjected to shallow or deep-seated soil (ground) movement. Depending on the geometry, geotechnical and climatic conditions in the slopes, these movements may be due to soil yielding, creeping, or failure. It is of practical importance to evaluate the effect of active ground movement on the structural integrity and serviceability of the pipelines in the moving slopes so that one can develop and implement an effective field monitoring and remediation program if necessary. Simplified design methods for pipelines subjected to longitudinal soil movements at shallow depth have been proposed and developed by several researchers (e.g., O'Rourke et al. 1995; Rajani et al. 1995; Chan and Wong 2004). In these methods, one of the major assumptions is the use of the axial soil spring model in the analysis of the deflected profile of the pipeline. The axial soil spring model is detailed in existing buried pipeline design guidelines (ALA 2001; PRCI 2009). However, these methods and guidelines do not consider the effect of excess pore pressure response around the pipe under varying axial loading rates. They recommend to use effective (drained) and total (undrained) soil parameters

to accommodate the slow and fast loading rates, respectively. In addition, the effect of time- or rate-dependency on soil strength parameters is not taken into account in the axial soil spring model.

This paper improves the aforementioned axial soil spring model and design method for pipelines subjected to axial loading by considering the effect of soil displacement rate on (i) excess pore pressure responses (generation and dissipation) around the pipe and (ii) soil-pipe interface behaviour. The proposed analytical tools allow one to assess if the pipeline yields in the critical locations of the slip. A case study is presented to illustrate the analytical procedures. It is important to note that the proposed method is only applicable for design of straight pipe sections. Analysis of side bend and vertical bend are beyond the scope of this paper. In addition, the proposed method does not take into account other loadings, such as transverse uplift and bearing loading, lateral loading, pipe internal pressure, thermally induced stresses, and corrosion that may govern the overall performance of the pipeline.

2 TRANSLATIONAL SLIP – AXIAL LOADING

Translational slips occur where the failure (slip) surface passes through a weak stratum at a relatively shallow depth or above the bedrock. For illustration, consider a translational slip in an infinite slope in which a pipe is buried at a shallow depth (Fig. 1). The pipe alignment is parallel to the slope which is a common practice. The direction of the translational slip is governed by that of the shear plane or bedrock. In such simple case of Fig. 1, the slide direction, pipe alignment and slope inclination are equal, defined by angle α such that the pipe is subjected to axial loading. Slope indicators are one of the sensors commonly used to measure the soil displacements. They are installed in vertically drilled boreholes to measure the soil horizontal displacements along the depth. The relationship between the slope indicator reading at the pipe, δ_{SI} and the soil displacement field around the pipe, δ_L is given as:

$$\delta_L = \frac{\delta_{SI}}{\cos(\alpha)} \qquad [1]$$

where α = inclined angle of the slope.

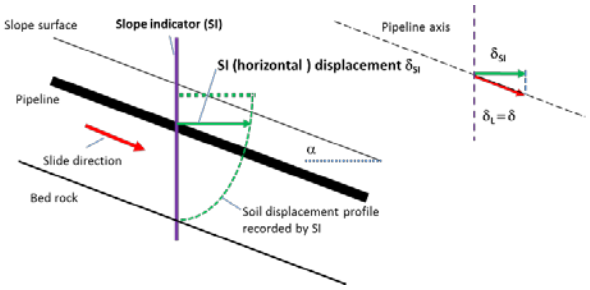

Fig. 1. Sketches showing the relationship among displacement monitored by slope indicator δ_{SI}, slope displacement δ, soil axial (longitudinal) component δ_L acting on the pipe

2.1 Stress equilibrium

For calculation of soil loading exerted on the pipeline, the soil displacement field around the pipe must be determined. Fig. 2 illustrates the evolution of idealized soil deflection profiles around a pipe in a progressive translational slip. Soil deformation around the pipe increases from state 'a' to state 'c' with increasing soil downward movement. A permanent slip initiates at state 'd' when the shear strength at the soil-pipe interface has been overcome. If the soil constitutive model is represented by an idealized perfectly elasto-plastic behavior as shown in Fig. 3a, the axial soil spring model may be equivalently described by the idealized relationship shown in Fig. 3b.

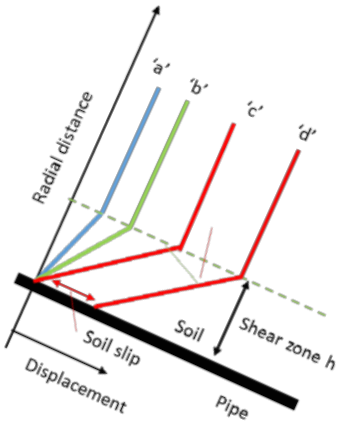

Fig. 2. Idealized soil displacement profiles and development of shear zone near the pipe with increasing soil displacement under axial loading

For a more realistic representation of soil behavior, a hyperbolic model developed by Duncan and Chang (1970) may suffice, which is given as:

$$\tau = \frac{\gamma}{\frac{1}{G_o} + \frac{\gamma}{\tau_u}} \qquad [2]$$

where γ = shear strain, G_o = initial shear modulus, τ_u = ultimate shear strength ($\tau_f = R_f \tau_u$); R_f = failure parameter less than unity, τ_f = failure shear strength ($\tau_f = c + \sigma' tan\phi$ where c and ϕ soil are cohesion and friction angle, respectively).

Considering the stress equilibrium state around the pipe under axial loading (Fig. 4), the shear stress distribution around the pipe may be of the form:

$$\tau = \tau_a \frac{a}{r} \qquad [3]$$

where τ = shear stress at a radial distance of r; τ_a = shear stress at the soil-pipe interface; a = pipe radius. Substituting the shear stress τ from [3] into [2], the shear strain distribution around the pipe may be obtained. Furthermore, the shear displacement distribution can

also be determined from integration of the shear strain distribution based on small-strain theory ($\gamma = du_r/dr$ where u_r is the shear displacement at r). The integral limits of $r = a$ and $r = 6a$ are used to yield approximate definite values within 10%. The effect of the free surface may affect the stress and strain distributions around the pipe.

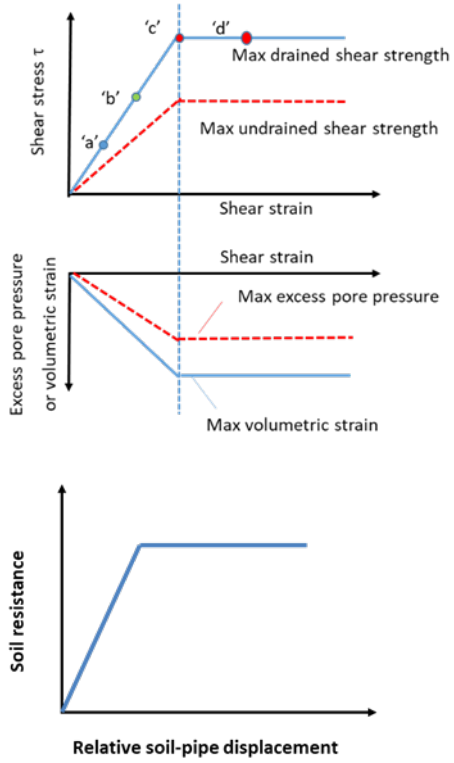

Fig. 3. (a) Idealized soil responses of shear stress, shear strain, volumetric strain and pore pressure under drained and undrained shearing in NC clay; (b) idealized relation between soil resistance and relative soil-pipe displacement

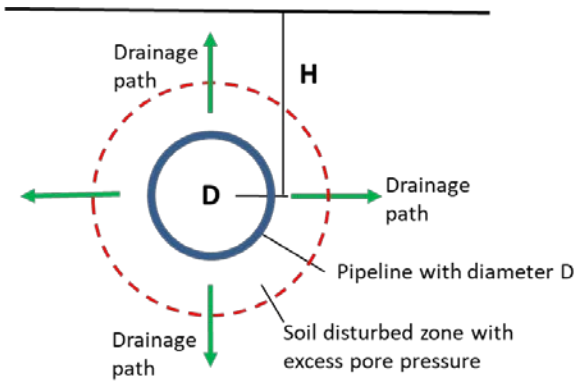

Fig. 4. Soil deformation and pore pressure response around the pipe subjected to axial (longitudinal) loading

Examples of normalized shear strain distributions around a pipe are shown in Fig. 5 for various values τ_a of 10, 50 and 95% of failure shear strength τ_f. The parameters of c = 30 kPa, ϕ = 21°, R_f = 0.9 and G_0 = 740 kPa were used in the example. The shear strain increases with increasing shear strength mobilization, and the concentration occurs at a zone of thickness less than 0.2a adjacent to the soil-pipe interface (Fig. 5) resulting in formation of a shear failure zone around the pipe.

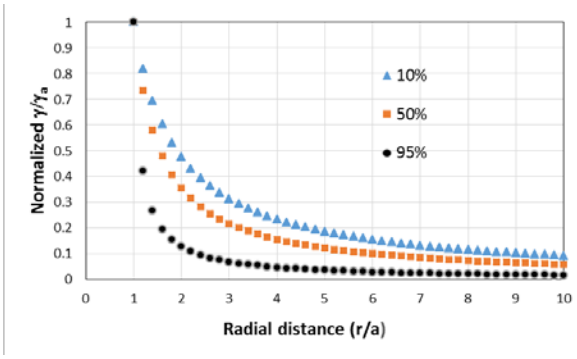

Fig. 5. Normalized shear strain around a pipe under 10, 50 and 95% of shear strength mobilization subjected to longitudinal (axial) loading - (γ_a and γ are shear strain at r = a and r, respectively; a = pipe radius)

2.2 Pore pressure responses

Based on the stress equilibrium analysis around the pipe, it is postulated that a shear failure zone of thickness h may occur around the pipe under axial loading (displacement) rate of $\dot{\delta_L}$ shown schematically in Fig. 2. This figure shows the evolution of idealized soil deflections or shear displacement profiles near the shear zone. Prior to state 'd' of the initiation of a permanent slip at the soil-pipe interface, the shear strain within the shear zone is γ, reached at time $t = \gamma h/\dot{\delta_L}$. The permanent slip occurs at $\gamma = \gamma_{max}$ or $t = t_f$ where $t_f = \gamma_{max} h/\dot{\delta_L}$. In this idealized model, it is assumed that the shear strain within the shear zone generates a shear induced (excess) pore pressure and this excess pore pressure is allowed to propagate outward under consolidation as illustrated as a radial flow problem in conjunction with Fig. 4. The excess pore pressure may be positive for contractile soil or negative for dilative soil.

The maximum excess pore pressure is a soil response depending on soil initial stress state and properties as shown in Fig. 6 under undrained shearing condition. For normally consolidated clay, the initial state NC(p_0, e_0) is on the 'wet' side of the critical state line. A positive shear induced pore pressure will be developed under undrained shearing, and its maximum magnitude is equal to the horizontal distance measured from its initial state to the state on the critical state line. For overconsolidated clay, the initial state OC(p_0, e_0) is on the 'dry' side of the critical state line. The shear-induced pore pressure under undrained shearing is negative due to its

dilative behaviour.

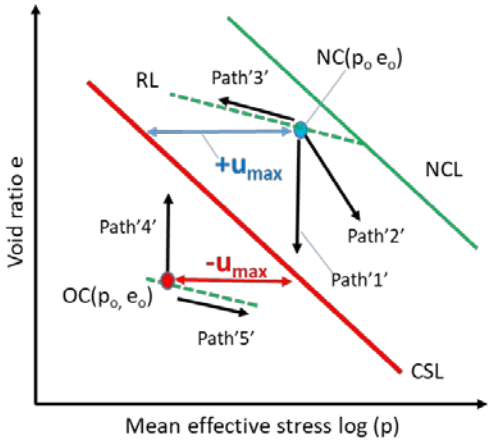

Fig. 6. Pore pressure responses inside and outside shear zone before full mobilization of maximum induced excess pore pressure u_{max}, maximum shear/volumetric strain in shear zone or permanent slip in the soil-pipe interface. NCL – normally consolidation line, RL – rebound line, and CSL – critical state line

First, consider the pore pressure response in normal consolidated clay under axial loading. The pore pressure responses within and outside the shear zone before and after γ_{max} or t_f may be determined considering the mass conservation of pore fluid within the porous medium. Before γ_{max} or t_f, excess pore pressure generation and dissipation occur simultaneously as illustrated in Fig. 7a. At $t = t_1$, the maximum excess pore pressure, $u_{max,t}$ denoted by area '1-2' is generated inside the shear zone. At the same time, consolidation inside the shear zone also takes place, and its degree of the consolidation is governed by the amount of pore water flowing out of the shear zone and into the adjacent zone. Thus, the area bounded by '1-2-3-4' inside the shear zone must be equal to the area under '4-5' outside the shear zone. Similarly, at $t = t_2$, the area bounded by '8-9-6-7' inside the shear zone must be equal to the area under '9-10' outside the shear zone. Assuming the total stress due to the overburden remains unchanged during the axial loading, the volume change inside the shear zone at time t, ΔV_s is given by

$$\Delta V_s = m_\lambda (u_{max,t} - u_s) V_s \qquad [4]$$

where m_λ = coefficients of compressibility in the shear zone; $u_{max,t}$ = maximum induced excess pore pressure in the shear zone at time t; u_s = excess pore pressure in the shear zone at time t; V_s = volume of shear zone per unit width ($V_s = 2\pi ah$); a = the pipe radius; h = thickness of the shear zone.

The volume change outside the shear zone at time t, ΔV_e is given by

$$\Delta V_e = m_\kappa (C_1 u_s) V_e \qquad [5]$$

where m_κ = coefficient of compressibility in the outer zone; V_e = the volume of the outer zone affected by excess pore pressure per unit width (integral volume of consolidating soil with linear excess pore pressure distribution with u_s at radial distance r = a + h, and zero at r = R, respectively; $V_e = 2\pi \left\{\frac{R^3}{6} - \left(\frac{R(a+h)^2}{2} - \frac{(a+h)^3}{3}\right)\right\}\left\{\frac{1}{(R-(a+h))}\right\}$; $R = \sqrt[n]{4\pi c_v t}$ for $R \geq a + h$ using the approximation of parabolic isochrones in consolidation-diffusion equation (Atkinson 1993); c_v = coefficient of consolidation; r = radial distance; n = constant (≈ 1); and C_1 = shape factor accounting for the non-linear excess pore pressure distribution profile (for 1D case, $C_1 \approx 0.67$; for radial case, $C_1 \approx 0.1$-0.3).

Equating [4] and [5] based on the principle of mass conservation and normalizing the excess pore pressure u_s with u_{max}, the following condition is obtained:

$$\frac{u_s}{u_{max}} = \frac{u_{max,t}}{u_{max}} \frac{1}{\left(\frac{m_\kappa}{m_\lambda} C_1 \frac{V_e}{V_s} + 1\right)} \qquad [6]$$

where u_{max} = the maximum induced excess pore pressure inside the shear zone in axial loading.

The coefficients of compressibility m_λ and m_κ and the value of u_{max} may be depicted from Fig. 6. For a normally or lightly consolidated soil following the critical state framework, the soil inside the shear zone may follow the stress path '1' in axial loading. Stress path '2' may be applicable to that encountered in other loadings such as transverse and lateral loading. The soil outside the shear zone should follow the path '3' along the rebound line (curve). The value of u_{max} is the horizontal distance between the initial in situ stress state (p_0, e_0) and the stress state on the critical state line in the e-p plot. For conservative estimation, u_{max} = p_0. In [6], the coefficients of compressibility may be expressed in terms of classical conventional parameters λ and κ which are dependent on the consolidation effective stress, p. Then, [6] becomes non-linear (Randolph et al. 2012). Randolph et al. (2012) assumed that the λ and κ coefficients are close.

At and after t = t_f, the shear stress at the soil-pipe interface (r = a) τ_a has reached its failure state τ_f. No additional excess pore pressure is generated in the shear zone, and the excess pore pressure will decay with pore fluid leaking into the outer zone. The pore pressure response inside and outside the shear zone may be illustrated in Fig. 7b. The mass conservation in pore fluid yields the following equation.

$$\frac{u_s}{u_{max}} = \frac{1}{\left(\frac{m_\kappa}{m_\lambda} C_1 \frac{V_e}{V_s} + 1\right)} \qquad [7]$$

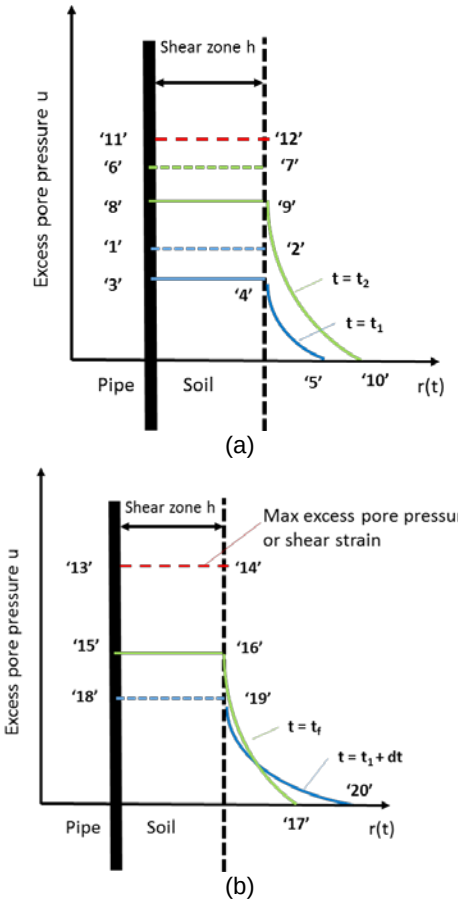

Fig. 7. Pore pressure responses inside and outside shear zone (a) before and (b) after full mobilization of maximum induced excess pore pressure u_{max}, maximum shear/volumetric strain in shear zone or permanent slip in the soil-pipe interface

Example relationships of [7] between normalized excess pore pressure inside the shear zone and normalized time or shear strain, are plotted in Fig. 8 for an assumed shape factor of C_1 = 0.2 and various ratios of $\frac{m_\lambda}{m_\kappa}$. One can use this plot to determine the degree of excess pore pressure dissipation with a given $\dot{\delta_L}$. In other words, this can be treated as a criterion for drainage condition for axial loading. For examples, $\frac{c_v t}{h^2}$ (or $\frac{\gamma_{max} c_v}{vh}$) of 200 and 1000 must be satisfied to maintain a drained condition of 95% consolidation for $\frac{m_\lambda}{m_\kappa}$ = 1 and 4.6, respectively. Lower $\dot{\delta_L}$ may result in lower excess pore pressure generation and higher degree of consolidation inside the shear zone. At a given $\dot{\delta_L}$, the excess pore pressure induced in soils with high $\frac{m_\lambda}{m_\kappa}$ is larger than that induced in soils with low $\frac{m_\lambda}{m_\kappa}$.

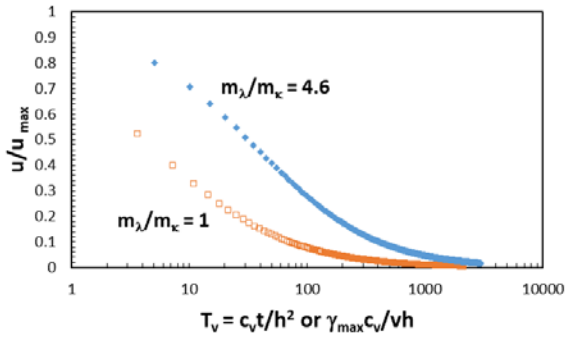

Fig. 8. Normalized excess pore pressure versus normalized time (or displacement rate) at the initiation of slip at soil-pipe interface

The excess pore pressure responses inside the shear zone as a function of time are illustrated in Fig. 9, for a given axial (longitudinal) displacement rate $\dot{\delta_L}$. The soil displacement continues to increase at a constant rate of $\dot{\delta_L}$. The excess pore pressure and shear strain inside the shear zone also increase at a constant rate under undrained condition, but will level off at and after γ_{max} or t_f. The consolidation process allows excess pore pressure dissipation under drained condition. The excess pore pressure inside the shear zone gradually increases to a peak at t = t_f, and decays thereafter. From [6] and [7], the excess pore pressure responses inside the shear zone are a function of displacement rate $\dot{\delta_L}$. Fig. 10 are schematics showing the excess pore pressure responses with varying $\dot{\delta_L}$. As expected, higher $\dot{\delta_L}$ results in higher excess pore pressure buildup. However, higher $\dot{\delta_L}$ may have an enhancing effect of the soil shear strength due to the time-dependent viscous behavior, which will be explored next.

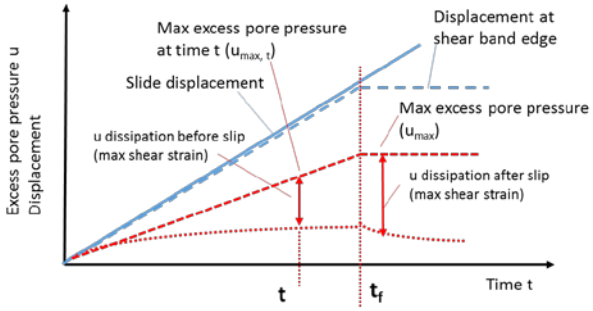

Fig. 9. Excess pore pressure responses in the shear zone or at soil-pipe interface before and after full mobilization of maximum induced excess pore pressure u_{max}, maximum shear/volumetric strain in shear zone or permanent slip in the soil-pipe interface

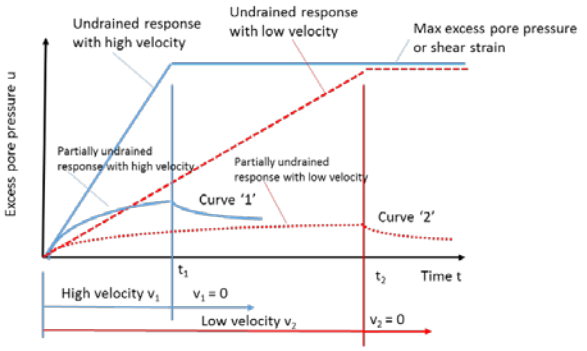

Fig. 10. Excess pore pressure responses in the shear zone or at soil-pipe interface for different soil displacement rates or velocities. Curves '1' and '2' represent for high (v_1) and low (v_2) soil displacement rates, respectively

The above illustrations and formulation for excess pore pressure responses inside and outside the shear zone in normally consolidated clay under axial loading may be extended to the responses in overconsolidated clay. For OC clay, the excessive pore pressure is negative or dilative, and its maximum magnitude is limited by its hydrostatic head equal to its overburden depth. The pore water is drawn into the shear zone according to the negative hydraulic gradient. The soil inside the shear zone experiences a shear dilation, and may follow the stress path '4' as illustrated in Fig. 6, while the OC soil outside the shear zone takes the stress path '5' along the rebound curve.

3 RATE-DEPENDENT (VISCOUS) SHEAR STRENGTH OF SOIL

In the axial soil spring model recommended by PRCI (2009), the axial (longitudinal) soil resistance equation comprises two main components, a soil cohesion-dependent and a friction-dependent component:

$$T_U = \pi D \alpha c + \pi D H \bar{\gamma} \left(\frac{1+K_0}{2}\right) \tan\delta \qquad [8]$$

where T_U = maximum axial (longitudinal) soil force per unit length of pipe transmitted to the pipe; D = outside pipe diameter; α = soil adhesion factor; c = soil cohesion, H = pipe embedment depth; $\bar{\gamma}$ = soil effective unit weight; K_0 = lateral earth pressure coefficient at-rest; and δ = soil-pipe interface friction angle depending on soil friction angle φ and pipe coating.

The soil parameters embedded in [8] are effective stress or drained parameters. Effective stress approach should be used to conduct geotechnical design and analysis of engineered structures if all the soil drained parameters are availably determined. The question is: how are these drained parameters influenced by the strain rate? In common practice, drained tests are preferable to undrained tests as the effect of shear induced pore pressure is insignificant. For low-permeability soils, the strain rate for the drained shearing condition is very low which may be beyond the test machine limit. High strain rate may cause shear induced pore pressure. In such case, the change in shear strength could be due to both the change in effective stress and the rate effect. It is important to separate the rate-dependent shear strength from the total undrained shear strength observed in the tests under high strain rate or undrained condition.

The rate-dependent undrained shear behaviour has been studied extensively using consolidated undrained triaxial compression tests (e.g., Casagrande and Wilson 1951; Richardson and Whitman 1963; Sheahan et al. 1996; Vaid and Campanella 1997). One of the advantages of CU tests is that any strain rate can be applied to the test sample under undrained condition. Semi-logarithmic correlations between the undrained strength and strain rate have been used (Soga and Mitchell 1996):

$$\frac{s_u}{s_{u0}} = 1 + m \log\left(\frac{\dot{\varepsilon}_a}{\dot{\varepsilon}_{a0}}\right) \qquad [9]$$

where s_u and s_{u0} = undrained shear strengths at the applied strain rates $\dot{\varepsilon}_a$ and reference strain rate $\dot{\varepsilon}_{a0}$, respectively; and *m* = material constant (*m* = 0.1 for $\dot{\varepsilon}_{a0}$ = 1%/hr; Kulhawy and Mayne 1980).

Wong et al. (2020) demonstrated that s_u can be interpreted in terms of Hvorslev strength parameters. The friction component is rate-independent, and the cohesion component may be expressed as a function of strain rate in a form similar to

$$c_{\dot{\varepsilon}_a} = c_{\dot{\varepsilon}_{ao}} + b \log\left(\frac{\dot{\varepsilon}_a}{\dot{\varepsilon}_{ao}}\right) \qquad [10]$$

where $c_{\dot{\varepsilon}_a}$, $c_{\dot{\varepsilon}_{ao}}$ = cohesion strengths at applied strain rates $\dot{\varepsilon}_a$ and reference strain rate $\dot{\varepsilon}_{a0}$, respectively; and b = material constant.

4 CASE STUDY OF A PIPELINE IN A SLOPE WITH VARYING DISPLACEMENT RATES

4.1 Case details

The pipeline to be examined is an existing one located in slopes at Pembina River Crossing, approximately 3 km east and 6 km south of the town Lodgepole, Alberta, Canada (Song 2007). This pipeline is part of NPS30 Western Alberta System Mainline. Fig. 11 shows the cross section of the slope site. The pipeline runs across a creek, which diverges into the North Saskatchewan River. The southern slope of the creek is between 1.3 – 17.7° whereas the northern slope is slightly steeper, 8.3 – 18.9°. The pipeline was built of X60 steel with 413-MPa yield strength. The pipe wall thickness and diameters are 15.9 and 762 mm, respectively. The cover depth of the pipeline varies in a range of 1.0 – 4.4 m with an average being 1.67 m. The pipeline length in the south slope is about 310 m.

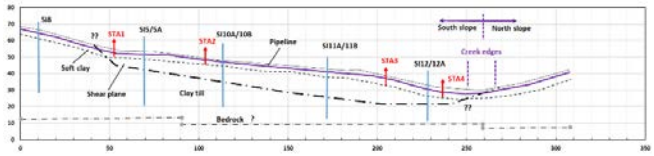

Fig. 11. Section showing details of pipeline, slope, shear slip plane, slope indicators (SI), and strain gauge stations (STA)

The soil stratigraphy at this site consists of a soft to stiff medium plastic silty clay and a stiff to firm low to medium plastic clay till. Underneath these surficial soils are interbedded claystone and sandstone formations. The thickness of the silty clay layer is about 1 to 4 m in which the pipeline was buried (Fig. 11). The clay till layer varies in a thickness of 30 to 60 m, containing sand lenses, laminated sand coal seams.

A rupture occurred in the original line after a rainfall in spring 1986. The original line was located at a site on the southern slope of the same creek in which active soil movements in the slope were observed. The existing pipeline is a re-route, constructed in the same year after the rupture, and is 0.5 km due west of the original crossing. After the re-routing, fifteen slope indicators were installed along the southern slope in respective years: 3 in 1987, 2 in 1988, 7 in 1992, and 3 in 1997. Some slope indicators were installed to replace the damaged ones. Based on geotechnical monitoring and analysis, two stress relief procedures were carried out in 1992 and 2000, respectively. Before the stress relief excavation in 2000, only four slope indicators were still functioning. Four new slope indicators were installed to monitor the soil movements in the southern slope before and during the stress relief procedure. The stress relief for the pipeline on the southern slope of the crossing took place in March 2000. A total length of 236 m of the buried pipeline was exposed by excavation, allowed to rebound to its non-stressed condition, and backfilled with excavated soil.

Data from nineteen slope indicators in the southern slope are available at different periods from 1988 to 2001 (Song 2007). All the slope indicators were installed in boreholes drilled at a distance of about 6-14 m away from the pipeline. In this study, representative data obtained from several slope indicators are presented to depict the evolution of soil movement pattern, and the profile of the shear planes developed in the southern slope of the crossing. Data from slope indicators SI-8, 10A, and 10B are presented in Figs. 12 – 13, and data of other slope indicators are summarized in Table 1. The reading data of the slope indicators reveal that the soil displacements along the downhill direction are dominant whereas those displacements perpendicular to the pipeline axis are minimal. Since the slope is quite gentle, the SI readings at surface is approximately equal to the longitudinal displacement δ_L.

Slope indicator SI-8 was installed at the crest outside the landslide. Over 20 years from 1992 to 2001, the soil movement rate is less than 1 mm/yr (Fig. 12). The soil displacement profile is characterized by a linear displacement pattern with depth and no distinct discontinuity.

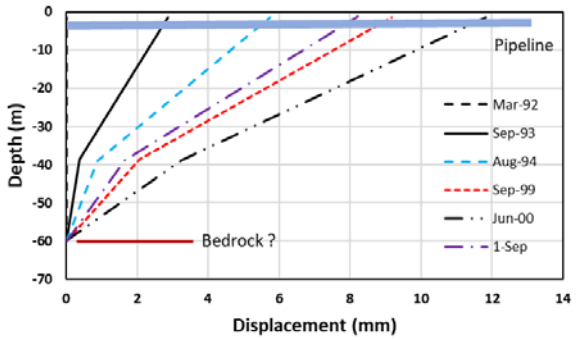

Fig. 12. Readings of slope indicator S-I8

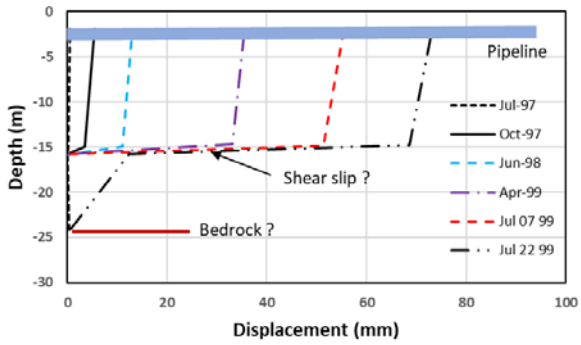

(a)

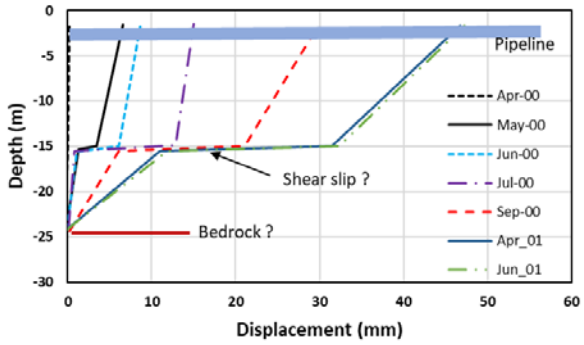

(b)

Fig. 13. Readings of slope indicators (a) SI-10A and (b) SI-10B

Table 1 summarizes details of soil displacements monitored by the slope indicators in the slope before the 1992 stress relief, between the 1999 and 2000 stress reliefs and after the 2000 stress relief, along with the years of installation and replacement. Prior to the 1992 stress relief, slope indicators SI-5, SI-6, SI-7 and SI-10 recorded soil displacements of 130, 89, 44 and 150 mm, respectively. Slope indicator SI-5 recorded the soil movement at the crest of the southern slope during the period of 1987 to 1999 (Fig. 11). It was replaced by slope indicator SI-5A before the 2000 stress relief. SI-5A

detected additional soil displacements of 90 and 28 mm before and after the 2000 stress relief. Slope indicator SI-10A was installed to replace SI-10 in 1997, and a soil displacement of 74 mm was monitored in 1997-99 (Fig. 13a). It was replaced by SI-10B before the 2000 stress relief. The soil displacement profile is characterized by a parabolic function of the soil displacement increasing with depth. A displacement discontinuity was detected at a depth of about 15 m from the slope surface (Fig. 13b). The soil displacement occurred at SI-10B after the 2000 stress relief is 48 mm. Slope indicator SI-11A was installed in 1997 and located near the middle portion of the landslide. It was replaced by SI-11B before the 2000 stress relief. The soil displacement profile is approximated by a rectangular pattern with depth. A slip might occur at a depth of about 20 m from the slope surface. The soil displacements recorded by SI-11A and SI-11B indicators before and after the 2000 stress relief are 12 and 42 mm, respectively. Slope indicator SI-12 was installed at a location when the shear plane was day lighted at the toe. The total soil movement during 1992-1997 is 150 mm. It was replaced by SI-12A before the 2000 stress relief. The soil displacement profile is characterized by a rectangular pattern with depth. A shear plane is likely to develop at a depth of about 12 m from the slope surface. The total soil displacement monitored at SI-12A is 75 mm. SI-12B was installed to replace SI-12A after the 2000 stress relief and a soil displacement of 42 mm was monitored until 2001.

Table 1. Different soil displacement rates recorded by slope indicators (Song et al. 2006)

Indicator ID	Installed in	Soil displacement before 1992 stress relief (mm)	Soil displacement between 1992 and 2000 stress relief (mm)
SI-8	1992	8	1
SI-5	1987	130	90
SI-5A	2000 (replacing SI-5)	-	-
SI-6	1988	89	-
SI-7	1988	44	-
SI-10A	1997	-	74
SI-10B	2000 (replacing SI-10A)	-	-
SI-11A	1997	-	12
SI-11B	2000 (replacing SI-11A)	-	-
SI-12	1992	150	
SI-12A	1997 (replacing SI-12)	-	75
SI-12B	2000 (replacing SI-12B)	-	-

Table 1. Continued

Indicator ID	Soil displacement after 2000 stress relief (mm)	Maximum recorded displacement rate (mm/year)
SI-8	3	2.6 (Sep 92-Aug 93)
SI-5	-	280 (Jul-Sep 99)
SI-5A	28	52 (Jun-Sep 00)
SI-6	-	240 (Jul-Oct 89)
SI-7	-	132 (Jul-Oct 89)
SI-10A	-	480 (Jul 1999)
SI-10B	48	108 (Apr 01-Jun 01)
SI-11A	-	16 (May 97-Jul 97)
SI-11B	42	64 (May 00-Sep 00)
SI-12	-	178 (Apr 97-Jun 97)
SI-12A	-	179 (Jul 99)
SI-12B	42	84 (Jul 00)

Several observations may be made based on data shown in Table 1. The slope has been moving continually, and the displacement rate varied from 2.6 mm/yr (SI-8) and 480 mm/yr (SI-10A). The slope indicators become nonfunctional and need to be replaced when the soil displacement exceeds a certain value depending on the location of slip plane and soil displacement profile. Two stress reliefs were conducted when the soil displacements occurred at the crest (SI-5) and toe (SI-12) of the slope became excessive. Combined axial and transverse loading may be dominant at these two critical locations of the active slope.

Strain gauge pods were installed at four stations in the southern slope along the crossing to monitor pipe strains before, during and after the 2000 relief (Fig. 11). At each station, 4 strain gauges were mounted on the outer surface of the pipe at orthogonal alignments, i.e., 90^{o} apart. Table 2 summarizes the average strain accumulation at the four stations, along with the soil movements monitored by slope indicators. The groundwater condition in the southern slope of the crossing was monitored using pneumatic and standpipe piezometers installed in different geological units since 1988. The pressure readings reveal that the surficial geological units were not hydraulically communicated. The water pressures in these units were in static equilibrium with the water table near the slope ground surface. However, water was locally recharged in downhill direction feeding the shear plane resulting in water pressure buildup after heavy precipitation in warm seasons. Investigation of the shear failure mechanism in this slope and its causes is beyond the scope of this study. The significant water pressure buildup along the shear plane, accumulation of water bodies and reduction of soil matric suction near the slope surface may be

attributed to the slope downhill movement.

Table 2. Average pipe strain accumulation recorded by strain gauges at stations and total soil movements recorded by nearby slope indicators during 2000 stress relief (Song et al. 2006)

Station	Average strain accumulated (με)	Period	Total soil movement (mm)
ST1	-53.87	July – November 2000	14 (SI-5A)
ST2	-50.91	July – September 2000	15 (SI-10B)
ST3	-43.78	July – September 2000	8 (SI-11B)
ST4	-80.56	July – September 2000	7 (SI-12B)

4.2 Assessment

Normalized excess pore pressure responses inside the shear zone were calculated from [6] for contractile and dilative behaviors with displacement rates of 2.6 and 48 cm/yr, and plotted versus normalized time in Figs. 14 and 15, respectively. Table 3 summarizes the input parameters for soil and pipe. In contractile soil (Fig. 14), the time required to reach γ_{max} for low $\dot{\delta_L}$= 2.6 cm/yr (given by $t_f = \gamma_{max} h/\dot{\delta_L}$) is much longer than that for high $\dot{\delta_L}$= 48 cm/yr. For t < t_f, the excess pore pressure induced by slow axial loading ($\dot{\delta_L}$= 2.6 cm/yr) is much lower than that induced by fast axial loading ($\dot{\delta_L}$= 48 cm/yr). For NC soil, the normalized excess pore pressure reaches 0.05 and 0.45 in slow and fast displacement rates of 2.6 and 48 cm/yr, respectively. After t_f, the shear induced pore pressure gradually decays back to its initial in situ value. The excess pore response inside the shear zone in dilative soil is negative instead of positive as illustrated in Fig. 15.

Now, the soil shear resistance on the pipe can be calculated from [8] for a given displacement rate $\dot{\delta_L}$. The rate-dependent cohesion is determined from [10]. The overburden effective stress term $H\bar{\gamma}$ is replaced by the overburden total stress minus the pore pressure (hydraulic head pressure plus shear-induced excess pore pressure). The shear resistances were calculated for contractile and dilative behaviors for displacement rates of 2.6 and 48 cm/yr, and plotted versus normalized time in Figs. 16 and 17, respectively. The behaviours of the shear stress development with time for NC and OC soils are very different because of the differences in pore pressure response. From practical perspective, the variation of shear resistance during axial loading is insignificant for low $\dot{\delta_L}$= 2.6 cm/yr because there is sufficient time for dissipation of excess pore pressure and the rate effect on the cohesion strength is small. The equation proposed by PRCI (2009) of [8] is valid for low displacement rates. For high $\dot{\delta_L}$= 48 cm/yr, the rate effect on the cohesion strength starts to play a dominant role. In addition, the negative excess pore pressure is built up in OC clay in a fast rate resulting in an increase in the effective confining stress. Since the minimum (negative) shear induced pore pressure occurs at t = t_f, the maximum shear stress develops at the same instant. The shear stress exerted on the pipe by high $\dot{\delta_L}$= 48 cm/yr could be increased by about 10% and 20% in NC and OC soils, respectively as compared to that by low $\dot{\delta_L}$= 2.6 cm/yr.

Table 3 Input parameters used in axial soil-pipe interaction under varying soil displacement rates (Song et al. 2006)

Pipe	
Diameter (a)	762 mm
Wall thickness (t)	15.9 mm
Length (L)	236 m
Burial depth (H)	1.67 m
Young's modulus (E)	200 GPa
Yield strength	413 MPa
Yield strain	2065 με
Soil	
Bulk unit weight	19.2 kN/m^3
In situ stress coefficient (K_0)	0.72
Friction angle (φ)	21.5^o
Adhesion factor (α)	0.5
Soil-pipe interface friction angle (δ)	14^o
Cohesion at reference rate ($\dot{\varepsilon}_{a0}$ =1 %/hr)	30 kPa
Rate-dependent parameter (b)	0.082
Coefficient of consolidation (c_v)	10 m^2/y
Compressibility coefficient (m_κ)	0.044
Compressibility coefficient (m_λ)	0.205
Maximum shear strain at failure (γ_{max})	10%
Maximum excess pore pressure (u_{max})	+9 kPa (NC soil); -17 kPa (OC soil)
Shear zone thickness (h)	10 cm

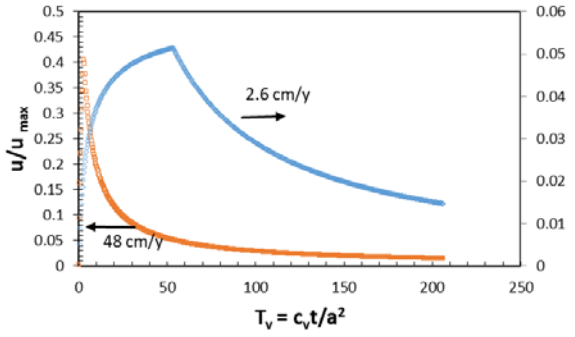

Fig. 14. Normalized excess pore pressure versus normalized time at the soil-pipe interface in normally consolidated clay under longitudinal (axial) loading at soil displacement rates of 2.6 and 48 cm/y

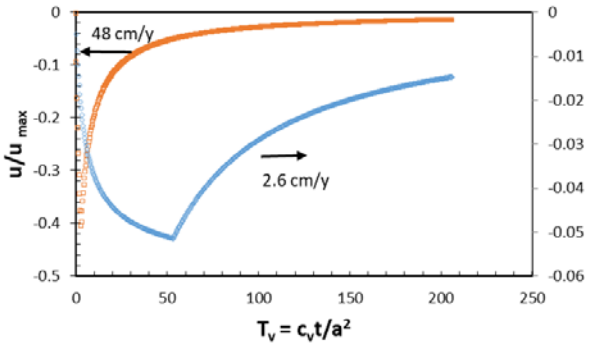

Fig. 15. Normalized excess pore pressure versus normalized time at the soil-pipe interface in overconsolidated consolidated clay under axial loading at soil displacement rates of 2.6 and 48 cm/y

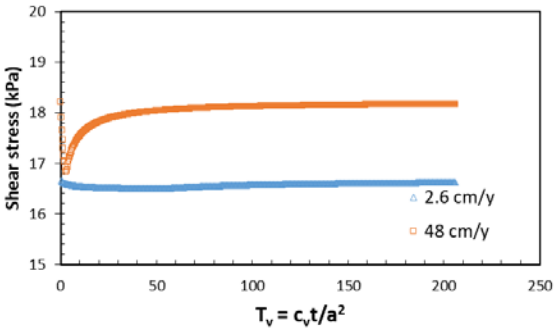

Fig. 16. Shear stress versus normalized time at the soil-pipe interface in normally consolidated clay under axial loading at soil displacement rates of 2.6 and 48 cm/y

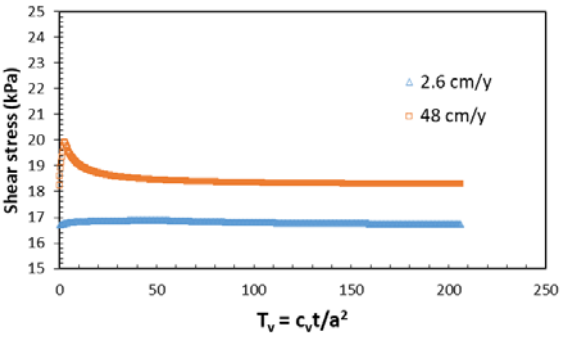

Fig. 17. Shear stress versus normalized time at the soil-pipe interface in overconsolidated clay under axial loading at soil displacement rates of 2.6 and 48 cm/y

The maximum strain exerted on the pipeline in a translational slip due to axial loading may be estimated from the equation given by Chan and Wong (2004). In this particular case, the soil ultimate resistance is mobilized along most of the pipeline length embedded in the unstable soil mass. The maximum strain induced in the pipeline at the slip edges ε_{max} is reduced to a simple expression that depends on the soil resistance properties, slip length, and pipeline dimensions:

$$\varepsilon_{max} = \frac{\tau_{max} L}{2Et} \qquad [11]$$

where τ_{max} = maximum soil shear stress on the pipe; E and t = pipe Young's modulus and wall thickness, respectively; L = the slip length. Equation [11] assumes that the lower and upper halves of the pipe length are under compression and tension, respectively.

With L = 236 m and other parameters listed in Table 3, the maximum strains were calculated for varying displacement rates in NC and OC soils and plotted in Fig. 18 for comparison. For NC soil, the maximum shear induced pore pressure occurs at t = t_f. Thus, the initial in situ pore pressure was used in the calculation of the overburden effective stress. For OC soil, the minimum (negative) shear induced pore pressure occurs at t = t_f. This negative value was used in the calculation of the overburden effective stress. The limiting soil displacement required to fully mobilize the maximum shear strain is about 10 mm with an assumed shear zone thickness of h = 100 mm and maximum shear strain γ_{max} of 10% (PRCI (2009) recommend 3 – 10 mm for stiff and soft soils). This limiting value increases with h and γ_{max}. The soil displacements monitored by slope indicators inside the slip are larger than this limit of 10 mm. Thus, soil-pipe interaction under axial loading of [11] is applicable for calculation of strain in the pipe, and results of Fig. 18 based on [11] could be used to predict the strain in the pipe for a given soil displacement rate $\dot{\delta_L}$. The strains in the pipe in OC clay are higher than those in NC clay. The strain in the pipe increases with increasing $\dot{\delta_L}$. In Pembina site, the clay till is an OC soil. The strain increases from 710 to 770 με for increasing the $\dot{\delta_L}$ from 2.6 to 48 cm/yr. The increase is about 9%, but the absolute strain in the pipe is still well below the yield strain or stress of the steel pipe. It appears that axial loading is not the key mechanism causing the pipe rupture which is consistent with the results of finite element simulation by Song et al. (2006). Combined axial and transverse loading on the pipe at critical locations where the slip surfaces daylight should be considered in future analysis. The stresses exerted on the pipe sections by the combined axial-transverse loading at the crest and toe of the slope are much more critical than those by the pure axial loading along the middle section of the slope. The 1992 and 2000 stress relief might have been an effective remedial method to relieve the stresses exerted on the pipe sections at the crest and toe of the slope.

It is of practical interest to compare the strain calculated from the guideline of PRCI (2009) with those estimated from the proposed method. Based on the input parameters listed in Table 3, the strain estimated from PRCI (2009) is 684 με. From Fig. 18, this value is comparable to those in NC soils with high displacement rates, but lower than those in OC soils. For OC soils with $\dot{\delta_L}$ of 48 cm/yr, the strain could be as high as 770 με. The discrepancy is attributed to the fact that PRCI (2009) does not account for the shear induced pore pressure and rate-dependent cohesive strength.

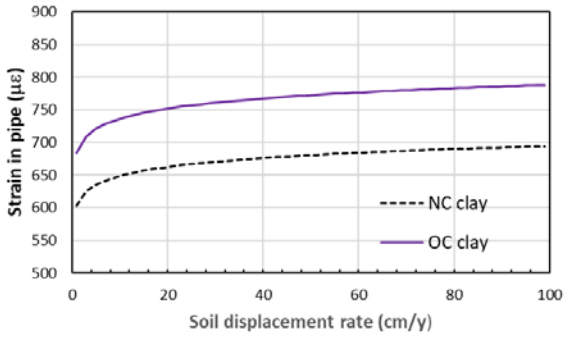

Fig. 18. Strain in pipe versus soil displacement rate in normally and overconsolidated clay under axial loading

5 CONCLUSION

This paper addresses the limitations in the use of existing design guidelines (ALA 2001; PRCI 2009) for buried pipelines in axial (longitudinal) loading. These guidelines do not consider the effect of excess pore pressure response and varying loading rate on soil-pipe interaction. For pipelines subjected to axial loading, a shear zone is developed around the soil-pipe interface. The maximum excess pore pressure generated within the shear zone is rate dependent. The higher the soil displacement rate, the higher the excess pore pressures is. This shear induced pore pressures are positive and negative for normally consolidated and overconsolidated soils, respectively. The axial loading rate also affects the soil cohesive strength, and thus the soil ultimate resistance and the maximum strain on the pipeline. Based on a case study on the performance of a pipeline at the Pembina River Crossing, the strain exerted on the pipe due to rate dependent axial loading may not be sufficient to exceed the pipe yield strain. The stress relief procedure is an effective method to mitigate the strains accumulated at the crest and toe of the slip where the combined axial and transverse loading may be dominant. Further investigations on rate effect on the combined axial and transverse loading are required.

ACKNOWLEDGEMENT

The authors appreciate the support provided by the Natural Science and Engineering Council of Canada (NSERC) and University of Calgary.

REFERENCES

American Lifelines Alliance (ALA). 2001. Guidelines for the design of buried steel pipe. www.americanlifelinesalliance.org.

Atkinson, J. 1993. Introduction to mechanics of soils and foundations. McGraw-Hill International (UK) Limited, 337 pages.

Chan, P.D. and Wong, R.C.K. 2004. Performance evaluation of a buried steel pipe in a moving slope: a case study. *Canadian Geotech. J.*, 41(5), 894-907.

Casagrande, A. and Wilson, S.D. 1951. Effect of rate of loading on the strength of clays and shales at constant water content. *Geotechnique*, 2(3): 251–263.

Duncan, J.M. and Chang, C-Y. 1970. Nonlinear analysis of stress and strain in soils. *ASCE Soil Mechanics and Foundation Division Journal*, 96(5): 1629-1653.

Kulhawy, F.H. and Mayne, P.W. 1990. Manual on estimating soil properties for foundation design. Final Report, Project 1493-6, EL-6800, Electric Power Institute, Palo Alto, CA.

O'Rourke, M.J., Liu, X. and Flores-Berrones, R. 1995. Steel pipe wrinkling due to longitudinal permanent ground deformation. ASCE *Journal of Transportation Engineering*, 121(5): 443–451.

PRCI (Pipeline Research Council International). 2009. Extended model for pipe soil interaction. Catalog No. L51990.

Rajani, B.B., Robertson, P.K., and Morgenstern, N.R. 1995. Simplified design methods for pipelines subject to transverse and longitudinal soil movements. *Canadian Geotech. J.*, 32(2): 309–323.

Randolph, M.F., White, D.J., and Yan, Y. 2012. Modelling the axial soil resistance on deep-water pipelines. *Geotechnique*, 62(9): 837–846.

Richardson, A.M., and Whitman, R.V. 1963. Effect of strain-rate upon undrained shear resistance of a saturated remoulded fat clay. *Geotechnique*, 13(3): 310-324.

Sheahan, T.C., Ladd, C.C. and Germaine. J.T. 1996. Rate-dependent undrained shear behavior of saturated clay. *J. Geotech. Eng.*, 22(2): 99–108.

Soga, K. and Mitchell, J. K. 1996. Rate dependent deformation of structured natural clays. Proc. ASCE Geotech. Special Publication No. 61, pp. 243–257.

Song, B., Cheng, J.R., Chan, D.H. and Zhou, J. 2006. Numerical simulation of stress relief of buried pipeline at Pembina river crossing. In Proceedings of the 2006 International Pipeline Conference, September 25-29, 2006, Calgary, Alberta, Canada: ASME, pp. 325-334.

Song, B. 2007. Effectiveness of the stress relief procedures and their effects on local buckling behaviour of buried pipes. PhD thesis, University of Alberta, Alberta, Canada.

Vaid, Y.P. and Campanella, R.G. 1977. Time-dependent behavior of undisturbed clay. *ASCE Journal of the Geotechnical Engineering Division,* 103(7): 693-709.

Wong, C.K, Li, B. and Wong, R.C.K. (2020). Viscous (time-dependent) behaviour of saturated clay in consolidated undrained triaxial compression. *GeoVirtual 2020* Resilience and Innovation, Calgary, September 14-16, Paper No, 54.